POLITECNICO DI TORINO
Repository ISTITUZIONALE

Enhanced Low-Voltage GaN FETs for e-Mobility Motor Control Improvements

Original
Enhanced Low-Voltage GaN FETs for e-Mobility Motor Control Improvements / Barba, V., Musumeci, S., Palma, M.. - (2023). (2023 AEIT International Conference on Electrical and Electronic Technologies for Automotive (AEIT AUTOMOTIVE) Modena, Italy 17-19 July 2023) [10.23919/aeitautomotive58986.2023.10217194].

Availability:
This version is available at: 11583/2991122 since: 2024-07-23T13:14:06Z

Publisher:
IEEE

Published
DOI:10.23919/aeitautomotive58986.2023.10217194

Terms of use:

This article is made available under terms and conditions as specified in the corresponding bibliographic description in the repository

Publisher copyright
IEEE postprint/Author's Accepted Manuscript

©2023 IEEE. Personal use of this material is permitted. Permission from IEEE must be obtained for all other uses, in any current or future media, including reprinting/republishing this material for advertising or promotional purposes, creating new collecting works, for resale or lists, or reuse of any copyrighted component of this work in other works.

(Article begins on next page)

10 October 2026

Enhanced Low-Voltage GaN FETs for e-Mobility Motor Control Improvements

Vincenzo Barba
DENERG-PEIC
Politecnico di Torino
Torino, Italy)
vincenzo.barba@polito.it

Salvatore Musumeci
DENERG-PEIC
Politecnico di Torino
Torino, Italy
salvatore.musumeci@polito.it

Marco Palma
Director, Motor Drive Systems and Applications
Efficient Power Conversion
Torino, Italy
marco.palma@epc-co.com

***Abstract*— Light e- Mobility plays an important role in the field of transportation. Recent studies show the advantages of adopting gallium nitride transistors (GaN FET) in low-voltage motor drive applications. This paper presents the benefits of choosing GaN FET technology for the electric powertrain. At first, GaN technology features are presented and compared to those of silicon-based (Si) transistors. Then, the typical e-powertrain layout with a GaN FET inverter is investigated through experimental tests. A focus on the DC-bus filter size and the dead-time selection is given. Advantages of using GaN FET have been found in terms of inverter output waveforms quality, system efficiency and power density, not only for the inverter but also for the filters and for the electrical motor. Finally, an overview of the emerging low-voltage motor drive applications is given. This work is useful for understanding how GaN FET operates, especially in motor drive applications in low voltage systems typically of light e-mobility.**

Keywords*— *GaN FET, Inverter, dead time, Light e-mobility, e-bike, power train.

I. INTRODUCTION

Among the wide bandgap (WBG) devices currently on the market, high electron mobility gallium nitride (GaN) transistors (HEMTs) are growing rapidly over silicon-based alternatives, such as super-junction transistors or Silicon Carbide (SiC) devices up to voltage ratings around 600V [1-3]. Benefits include significantly lower input and output capacitances (C_{ISS}, C_{RSS} and C_{OSS}), resulting in lower switching losses. Also, the Miller capacitance of a GaN transistor is much lower than a MOSFET with comparable $R_{DS(ON)}$ [4]. Thus the GaN device can be turned on and off much faster, which, in turn, allows for the use of smaller transformers and passive components. Additionally, lower input resistance per unit area leads to reduced conduction losses. Furthermore, the switching frequency in hard-switching operation is extended up to tens of MHz [5]. In low-voltage applications (≤200V), GaN technology is more competitive compared with Silicon (Si) MOSFET [6] and allows for obtaining high-performance power converters with reduced volume. The increasing of the switching frequency with reduced power losses leads to high-efficiency power converters with decreased size very profitable for autonomous battery systems. In this kind of emerging power electronic applications, the light e-mobility such as electric bikes (e-bikes), electric kick scooters or Unmanned Aircraft Systems (UAS); are more attractive for the GaN technology application [7], [8]. Furthermore, several low-voltage automotive applications of power converters regarding the charger circuits and the motor control for the fan, power steering and starter-alternator [9]. In the paper, an overview of the low-voltage inverter for motor control applications in light e-mobility and automotive applications implementing GaN FET devices is carried out. The GaN FET in motor control is investigated by comparing the specific technology and dynamic characteristics with Si MOSFETs. The GaN FET impacts on the inverter in output and input experimental waveforms improvements are explored, and the benefits of the HEMT devices are highlighted. Several GaN-based experimental inverter boards' performances are discussed.

II. GAN TECHNOLOGY FOR MOTOR CONTROL

Nowadays, GaN FET technology is becoming more and more popular in low voltage (48 V – 600 V) applications, and it is on the way to substituting Silicon transistor technology (MOSFET). GaN FET benefits are most significant in terms of switching losses and package size. Thus it performs at a higher power density than MOSFET. This is a result of GaN FET features that make this technology special and attractive.

Parasitic capacitances determine the commutation dynamic. Their values change non-linearly with the applied drain-source voltage [10]. Fig. 1 shows the GaN FET model with parasitic capacitors, inner gate resistor and the equivalent body diode in Fig. 1a and the behaviours of the parasitic capacitances versus the drain to source voltage in Fig. 1b. As example, those of GaN FET featuring $R_{DS(on)}$=3.6 Ω on-resistance (EPC2065 from EPC) are presented.

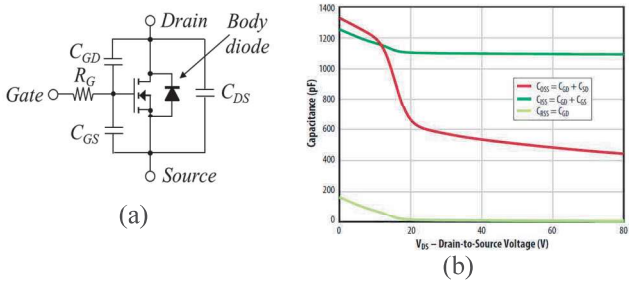

Fig. 1.(a) GaN FET model with parasitic capacitors, inner gate resistor and equivalent body diode symbol. (b) Parasitic capacitors behaviour versus drain-source voltage (V_{DS}) variation.

For example, two devices with 80 V breakdown voltage and similar on-resistance are compared. In Table I, the input capacitance $C_{ISS} = C_{GS} + C_{GD}$ value and the output capacitance $C_{OSS} = C_{DS} + C_{GD}$ value measured at 0 V and 48 V of the considered GaN FET and of a MOSFET featuring $R_{DS(on)}$=2.6 mΩ on-resistance (BSC026N08NS5 from Infineon) are reported.

978-88-87237-37-3 ©2023 AEIT

TABLE I
GAN FET VS MOSFET CAPACITANCE COMPARISON

	$C_{ISS\ 0V}$ $[nF]$	$C_{ISS\ 48V}$ $[nF]$	$C_{OSS\ 0V}$ $[nF]$	$C_{OSS\ 48V}$ $[nF]$
GaN FET	1940	1610	2700	1025
MOSFET	6800	5200	5100	1100

From the comparison, it arises that the GaN FET has lower parasitic capacitances than the MOSFET.

The Total Gate Charge (Q_g) is the amount of charge that needs to be injected into the gate electrode to turn on the enhanced device. GaN FET has the advantage of having a lower Q_g value in comparison to the MOSFET. The GaN FET feature a Q_g=15 nC, while the MOSFET has Q_g=74 nC.

The lower capacitances and gate charge values of the GaN FET make it faster to turn on and turn off.

The inverter configuration is composed of three H-bridge configurations made of two devices, the high side and low side working complimentary. During switching, a dead time where both devices are driven off is mandatory to avoid shoot-through but introduces power dissipation for every switching transient. Dead time length is arbitrary and has to be chosen according to the device's features.

The MOSFET features a reverse recovery charge Q_{rr} of 92 nC, which causes a growth of the switching losses. In three phase inverter application, 48 V bus voltage and 100 kHz switching frequency f_{sw}, the MOSFET power dissipation introduced by Q_{rr} contribute to the power dissipation.

GaN FETs do not present the reverse recovery phenomenon because they do not feature a p-n junction [4], [11]; anyway, it acts as a diode if reverse polarized. This characteristic allows the completion of the turn-off transients faster and with lower losses in comparison with the Si-based technology.

On the other hand, when reversing polarized, GaN FET reverses conduction voltage drop V_{RC} is bigger than the MOSFET one [12]. For example, the datasheet of the BSC026N08NS5 reports a V_{RC}=0.85 V, while it is V_{RC}=1.5 V for the GaN FET. Fig. 2 shows the comparison of the overall power dissipation of the MOSFET in blue and of the GaN FET in green as a function of the dead time length for I_0=10 A in Fig. 2a and for I_0=30 A in Fig. 2b.

GaN FET higher V_{RC} causes the steeper slope of the GaN FET losses graph. Nevertheless, MOSFET reverse recovery losses grow with the current magnitude and the dead time length, tending to a constant value. Overall, GaN FET is more efficient at low dead time values. Moreover, a shorter dead time and lower power dissipation is achievable using the GaN technology [13].

GaN FET high reverse conduction voltage amplitude must be considered when defining the dead time. Its lengthiness must be long enough to allow the C_{OSS} charge/discharge dynamic but not too long to minimize the reverse conduction losses.

III. POWER TRAIN FOR LIGHT ELECTRICAL VEHICLES ISSUES

In the field of motor control, single-phase and multi-phase DC-AC converters are required. The motor drive system layout is typically composed of a battery, LC filter, inverter, electric motor (E-Motor), microcontroller and battery management system (BMS) and is shown in Fig. 3.

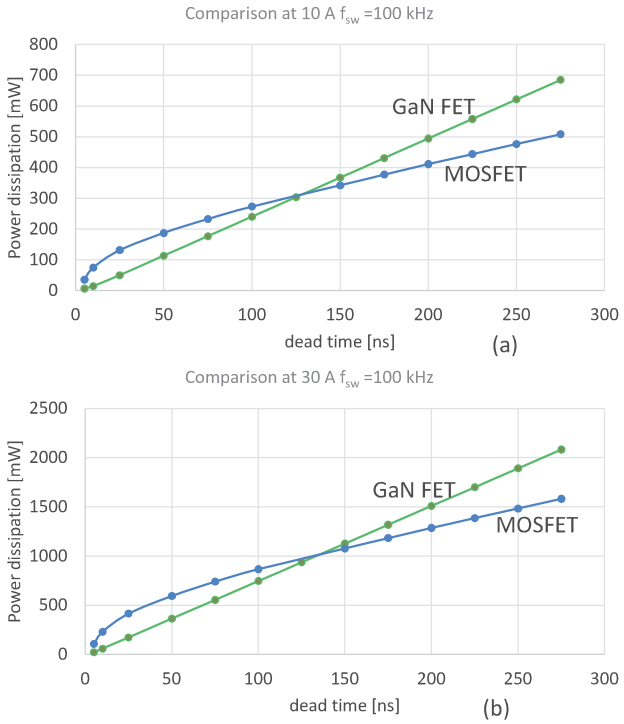

Fig. 2. Reverse conduction power losses at two current I_0 values versus the dead time length. Dead time range 5-275 ns. a) I_0=10 A. b) I_0=30 A

The BMS controls the battery state of charge and communicates with the microcontroller, which elaborates the PWM according to the E-Motor mechanical speed, rotor position and the measured currents.

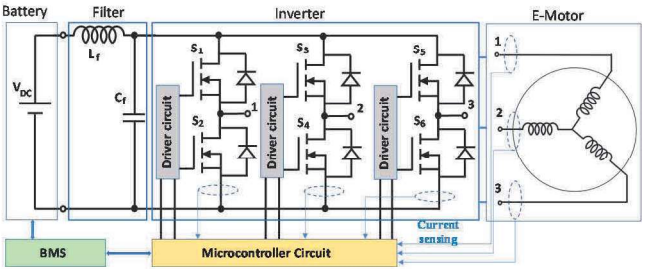

Fig. 3. system layout composed by battery, LC filter, inverter, electric motor (E-Motor), microcontroller and battery management system (BMS).

GaN FET can operate at switching frequencies higher than 100 kHz because of the fast switching transient. The high switching frequency reduces the ripple on the current waveforms that go to the motor and in the LC filter connected to the battery. A current waveform with less ripple minimizes the torque ripple, and motor efficiency arises [14]. Moreover, the high switching frequency has the benefit of reducing the LC filter size. In this way, it is possible to use ceramic or tantalum capacitors, thus avoiding the use of ceramic technology, which is less reliable.

A. DC link size reduction

The DC-link capacitor balances fluctuating instantaneous power exchange between the battery and the inverter. The DC-Link capacitor stabilizes the "ripple" caused by the inverter's high-frequency power switching circuits. In the system performance, a reliable and small-size DC-link capacitor plays

a key role. A test on a DC Brushless motor with phase current $I_{1,2,3}$ =I_o= 5 A, input voltage V_{DC}=36 V, switching frequency f_{sw}=100 kHz, and dead time 21 ns has been done. Fig. 4a shows the motor phase periodical waveform in a current period and the current ripple I_D. The resulting current and voltage waveforms are reported in Fig. 4 when using electrolytic filter capacitors (Fig. 4b), ceramic filter capacitors (Fig. 4c) and tantalum filter capacitors (Fig. 4d).

The comparison in Fig. 4 shows that at 100 kHz switching frequency, the same peak-to-peak ripple is obtained in the input voltage waveform using different C_f values and technologies. Ceramic capacitors are capable of handling high voltages. Furthermore, they feature low ESR and equivalent series inductance (ESL) with volume substantially reduced. Tantalum capacitors have high capacitance density; smaller package sizes are more easily obtainable than Aluminum electrolytic capacitors [8]. They have lower leakage currents and stability characteristics at a higher cost. The test demonstrates that such a high switching frequency, achievable with GaN FET technology, has benefits on the DC-link size, volume and cost reduction.

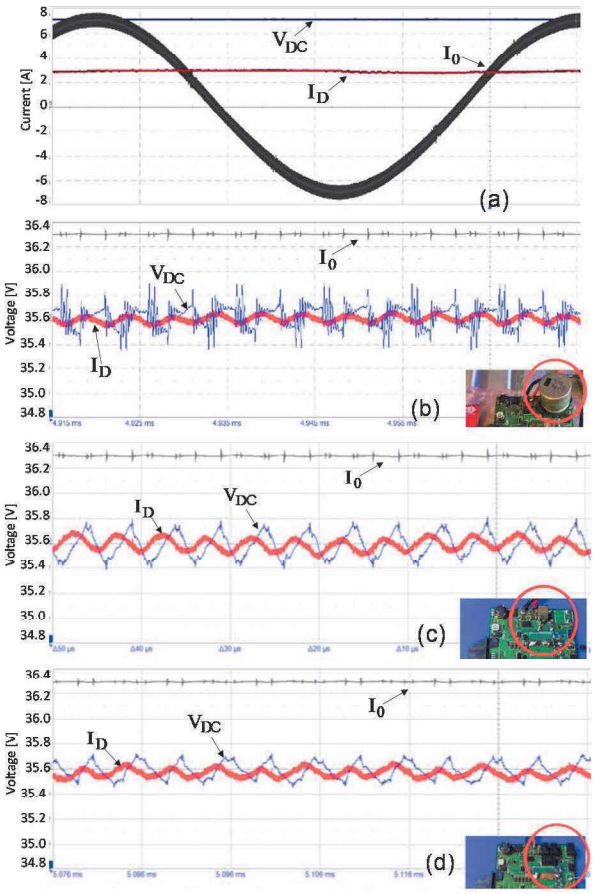

Fig. 4. Input voltage V_{DC}, phase current I_0 and current ripple I_D waveforms with different filter capacitor technologies: (a) periodical motor waveforms; (b) electrolytic capacitor C_f=660 µF; (c) ceramic capacitor C_f=22 µF; (d) tantalum capacitor C_f=30 µF.

B. *Torque ripple reduction*

The inverter PWM is able to generate an almost sinusoidal current waveform with modulation frequency f_m, performing a square phase voltage at a higher frequency f_{sw} and with a proper duty cycle. However, the current waveform presents some distortion in respect of a sine curve. In motor drive, the current distortion causes torque ripple and shaft vibrations. These can be limited using a very high f_{sw}/ f_m ratio. Moreover, the inverter dead time also causes a discontinuity when the current is close to a magnitude of 0 A.

A test where an inverter is connected to a DC Brushless motor with phase current $I_{1,2,3}$ =I_o= 5 A, input voltage V_{DC}=36 V, switching frequency f_{sw}=100 kHz has been done. The modulation frequency is f_m=22 Hz. Fig. 5 shows the phase current I_0 waveform and the resulting discrete Fourier spectrum when the dead time is 500 ns (Fig. 4a) or 14 ns (Fig. 4b).

Comparing the two operating conditions, arises that the current distortion is minimized using 14 ns of dead time. Moreover, the Fourier spectrum referring to the lower dead time length presents a great attenuation of the frequencies close to the principal one (22 Hz).

Such a short dead time value is achievable only by using an inverter with GaN FETs in the power stage because of the very fast switching transient.

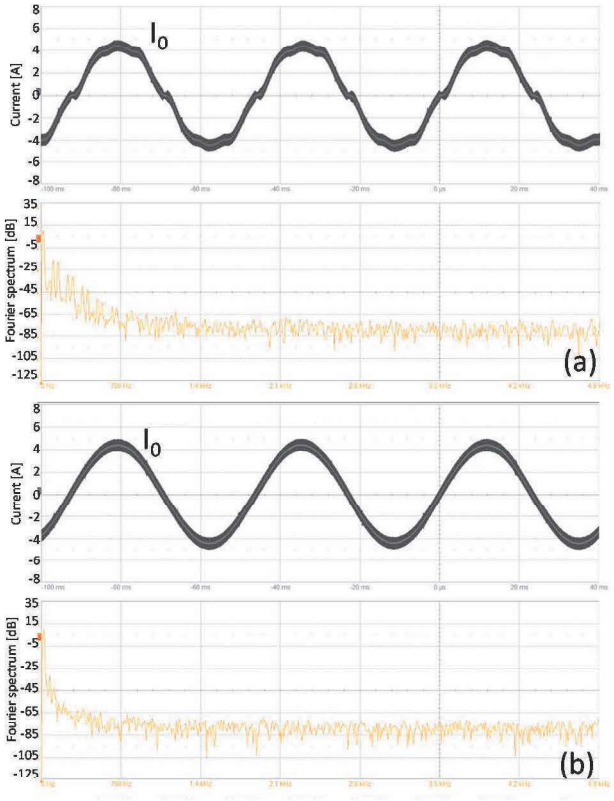

Fig. 5. phase current I_0 waveform and the resulting discrete Fourier spectrum: (a) dead time of 500 ns. (b) dead time of 14 ns. Timestep 20 ms. Frequency step 700 Hz.

IV. Low-Voltage Motor Drive Applications

Several boards have been designed for different applications, using proper discrete GaN devices or integrated power stages. The different boards evaluated are shown in Fig. 6.

A. *E-bike Motor Drive*

In city transport, e-bikes are affordable for sustainable mobility and its market is seeing a huge request in recent years and it is still growing. The technology of the power switches is crucial to obtain an efficient and reliable inverter system. E-bike powertrain works with low DC voltage, 24 V – 48 V

typically, and DC brushless for a strictly economic or permanent magnetic sinusoidal motor (PMSM) for more qualitative movement applications. In the field of light e-mobility application, GaN FET is the best candidate for realising the inverter power stage. For this porpoise, a GaN-based two-level inverter board has been used (EPC9167 from EPC). It uses a discrete GaN FET for each switch position. The adopted GaN FET is automotive qualified and features $R_{DS(on)}$=3.2 mΩ maximum, 80 V maximum device voltage (EPC2218A from EPC).

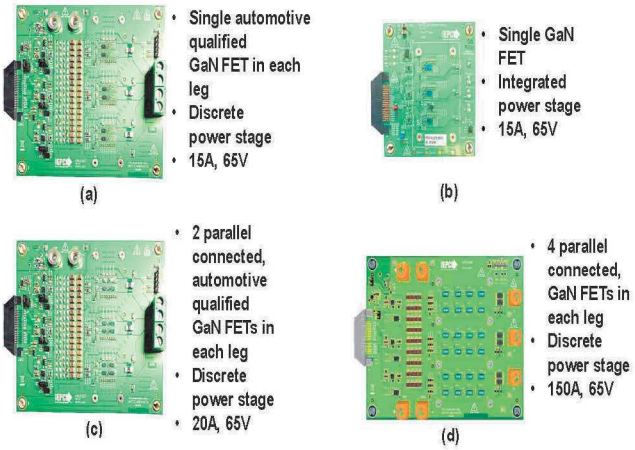

Fig. 6 Inverter boards designed for motor driving applications: (a) IC device; (b) Single discrete device; (c) 2 parallel connected discrete devices; (d) 4 parallel connected discrete devices.

The motor drive board is tested to work with a PWM switching frequency of f_{sw}=100 kHz and a DC input voltage of 48 V. The modulation frequency is f_m=5 Hz and works with a sinusoidal phase current of 10 A peak. 50 ns dead time are used. Fig. 7a shows the phase motor voltage V_0 in green and the phase current I_0 in yellow. The zoom toward the current peak is reported in Fig. 7b.

Fig. 8 shows the commutation transient of the low side turn-on (Fig. 8a) and of the high side turn-on (Fig. 8b) when the phase current reaches the 10 A peak magnitude. When the current goes from the phase motor to the inverter leg switching node, the commutation of the low side turn-on is faster than the high side one. In fact, in Fig. 8a, the voltage falls completely in almost 50 ns, while in Fig. 8b, the voltage rises in two steps: in the first one, it rises with a slope of 2.5 V/ns; then, it rises to 48 V as a step because the high side turns on in hard switching. This difference is due to the presence of the parasitic capacitance. During the low-side turn-on, the phase current can immediately pass through the GaN FET equivalent diode as the high-side device turns off. In this case, reverse conduction is present after the quick voltage variation. On the other hand, when the low-side device turns off, the phase current circulates through the parasitic output capacitance C_{OSS} that charges. Reverse conduction happens only after the C_{OSS} completes charging. In the case of Fig. 8b, 50 ns of dead time is not long enough for completing the C_{OSS} charging, so hard switching happens, avoiding the reverse conduction phenomenon.

The graph in Fig. 9 shows the case-to-ambient Δ-temperature in the function of the RMS phase current I_0 in the cases with switching frequency of f_{sw}=50 kHz or f_{sw}=100 kHz and by using a heatsink for air cooling or not. The graph shows that growing f_{sw} increases the temperature. A heatsink can help in limiting the temperature rising.

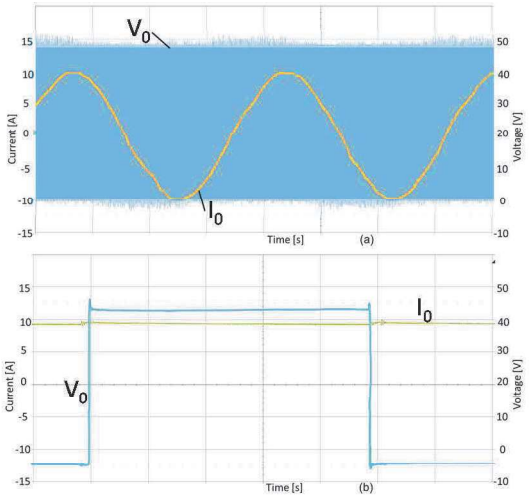

Fig.7. Phase voltage V_0 and current I_0 waveforms of the board designed for E-bike motor drive. (a) full sinusoidal period at 5 Hz; timestep 50 ms.(b) zoom on the switching period; timestep 2 µs.

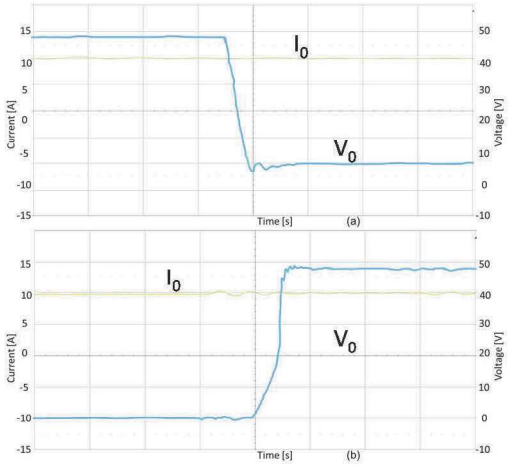

Fig. 8. Phase voltage V_0 and current I_0 waveforms during commutation of the board designed for E-bike motor drive: (a) low side turn-on. (b) high side turn-on. Timestep 100 ns/div.

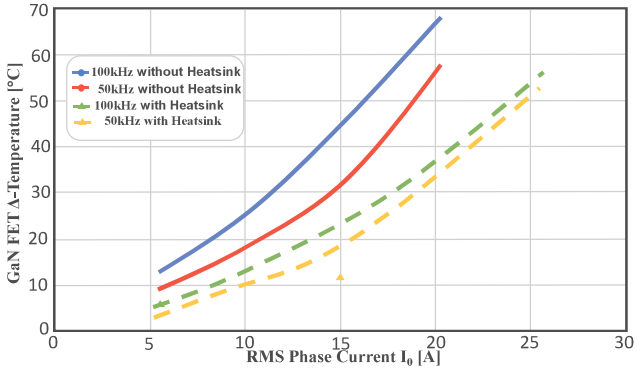

Fig. 9. GaN FET case-to-ambient Δ-temperature in function of the phase current I_0 of the board designed for e-bike motor drive. Switching frequency of fsw=50 kHz or fsw=100 kHz. Using a heatsink for air cooling or not.

B. Reduced Volume Motor Drive Applications

The volume reduction is a crucial design constraint in portable battery powered system. The integration of the power stage in converter applications is oriented to a significant inverter board size reduction. In Fig. 6b the inverter board

(EPC9176 from EPC) is designed to minimise the volume and increase the reliability. Comparing the area size of this board with the equivalent PCB layout of the inverter in Fig. 6a, the savings is about 50%. The inverter board consists of a motor drive inverter board based on a Power Stage IC ($R_{DS(on)}$=6.6 mΩ maximum, 100 V maximum device voltage. (EPC23102 from EPC). The 3-phase inverter is designed to supply electrical motor working in several volumes-save applications such as e-bikes, electric kick scooters and automotive fan drives. The experimental board can deliver a steady state phase peak current up to 27 A (20 A_{RMS}). The board supports PWM switching frequencies up to 250 kHz in motor drive applications and 500 kHz in DC-DC applications. It is an integrated power stage (IC) that integrates input logic interface, level shifting, bootstrap charging, and gate drive buffer circuits along with eGaN output FETs. With such IC, the number of components in the board is very reduced. This is a benefit for the PCB layout and reliability.

This inverter board has been tested, powering a brushless motor (BLDC) of 500 W. The inverter I supplied by 48 V DC input voltage and worked a PWM having a sinusoidal reference with a modulation frequency of f_m=5 Hz and a switching frequency of f_{sw}=100 kHz. The motor phase RMS current is 20 A. Fig. 10 shows the phase current and the measured board temperature in the described working operation.

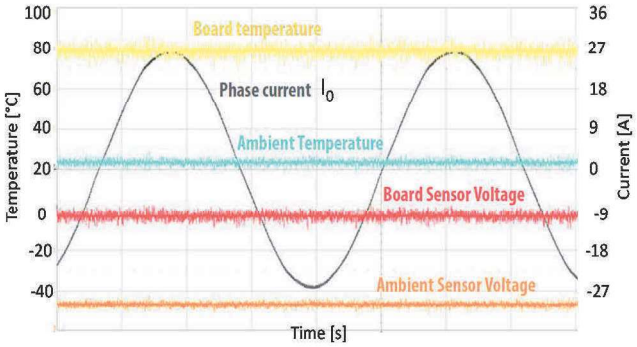

Fig. 10. Phase current I_0 and temperature sensor voltage of the board designed with IC GaN FET. Timestep 50 ms/div.

Test results reveal that the board temperature increases to 80°C when the ambient temperature is 26 °C. So, the board is thermally stable when working in an operation that performs very high-quality current waveforms.

C. E-Scooter Motor Drive

Micro mobility is a variegated, and not yet standardized electric mobility scenario made up of several relatively small battery-powered vehicle systems with autonomy ranges depending on many factors, such as weight, maximum torque, speed, number of people to move, safety, and cost. Electric scooters (e-scooters) belong to micro-mobility, but the motor torque request may require a current level that is too high for being conducted by a single device.

A solution to avoid damage in the converter due to the high current request is to use more FETs in parallel. In this way, the load current is subdivided between the power devices. For this purpose, the 3-phase inverter (EPC9167HC from EPC) has the power stages composed of two GaN FETs (EPC2218A from EPC) in parallel. The considered board is reported in Fig. 6c, and it is an evolution of the one in Fig. 6a. The board can deliver up to 42 A peak (30 A RMS) maximum output current.

The electric schematic of the inverter board with two parallel devices in each switching leg is depicted in Fig. 11.

The board is tested by powering a 500 W motor with a sinusoidal modulation frequency of f_m=5 Hz and delivering to the motor a phase current of I_0=25 A RMS. The input voltage is V_{DC}=48 V, and the PWM is realized with a switching frequency of f_{sw}=100 kHz and a dead time of 50 ns. Fig. 12 shows the phase current I_0 waveform and the board temperature measured with a thermal sensor.

The test reveals that the board is able to supply a high phase current with very low distortions and remains inside the thermal limits.

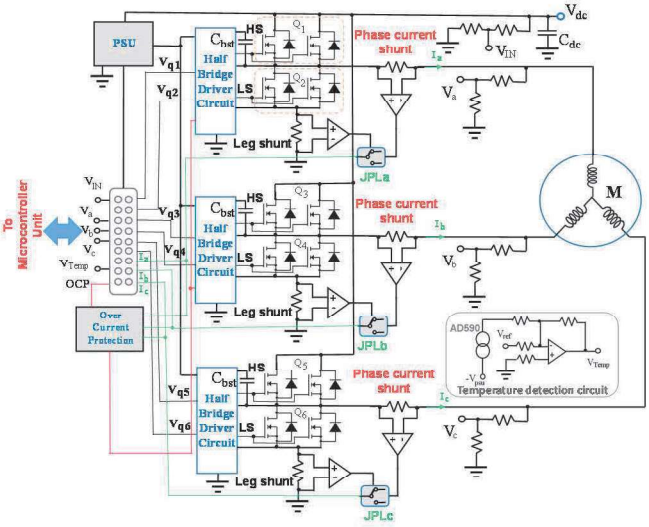

Fig. 11. Electric schematic of the inverter board with two parallel devices in each switching leg.

D. Starter Alternator

In vehicles, the starter motor and alternator are essential components.

The starter motor is basically a DC electrical machine or a permanent magnet machine directly supplied by the vehicle battery. During the cranking phase, the starter is mechanically connected to the Internal Combustion Engine (ICE) shaft and applies torque to accelerate the ICE. The torque request during cracking can be very high, and the inverter must be able to deliver a high current request. The alternator is an onboard electrical generation done with an electrical machine coupling the ICE shaft. An AC/DC converter rectifies the AC motor current to charge the battery. When a speed variation happens in a short time, the current magnitude can reach high levels.

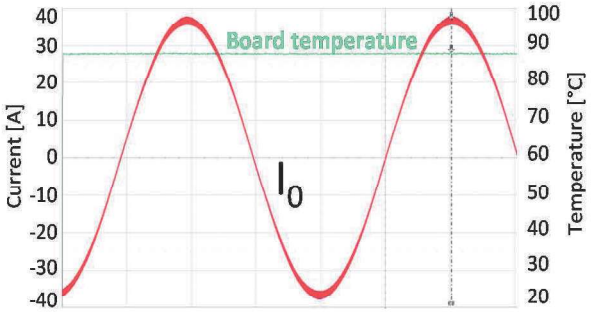

Fig. 12. Phase current I_0 and sensor board temperature of the board designed with 2 Parallel Connected Discrete GaN FETs. Timestep 50 ms/div.

For supplying higher currents, more than two parallel connected devices can be used. The designed board is a two-level inverter (EPC9186 from EPC) having four GaN FETs connected in parallel per switch position. The GaN FET has a conduction resistance of $R_{DS(on)}$=1.8 mΩ maximum $R_{DS(on)}$, 100 V maximum device voltage and can conduct a steady state current up to 100 A (EPC2302 from EPC).

This inverter board has been designed to work in safe operating conditions, with a phase current up to 150 A.

The board is tested when it supplies a motor working a PWM with a switching frequency of f_{sw}=100 kHz and 50 ns of dead time. The inverter input voltage is V_{DC}=60 V, and the phase current magnitude is I_0=150 A. Fig. 13 shows the phase current I_0 and the phase voltage V_0 waveforms. Fig. 13a focuses on some switching periods. The zoom toward the low side turn-on transient is depicted in Fig. 13b, while the high side turn-on transient is depicted in Fig. 13c.

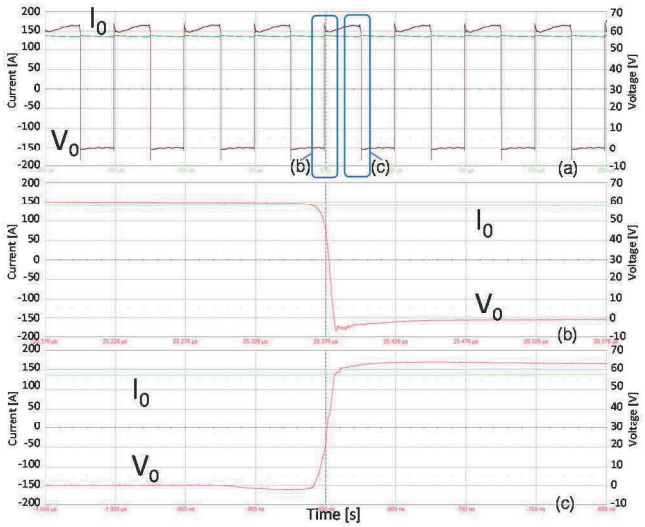

Fig. 13. Phase voltage V_0 and current I_0 waveforms during commutation of the board designed with four parallel connected discrete GaN FETs: (a) more switching periods, timestep 50 µs. (b) low side turn-on. (c) high side turn-on, timestep 50 ns/div.

V. Conclusions

In the paper, the use of GaN technology in DC-AC power converters for low-voltage light e-mobility power trains and automotive inverters for different auxiliary motor control applications is investigated, giving an overview of several applications. GaN FET is more attractive in inverter applications for the advantageous improvements in reducing the current ripple of the output waveforms and DC-link capacitances reduction caused by the higher switching frequency compared with Si MOSFETs. The quality of the output current is influenced positively by the dead time length significant reduction due to the device's input parasitic capacitors values decreasing with respect to the equivalent Si MOSFET devices. Furthermore, the device sizes and the high switching frequency allow a noticeable converter volume reduction. The converter system volume reduction and improved efficiency are crucial features for the application in modern autonomous battery systems, such as the e-bike or e-scooter, which are in great expansion on the sustainable e-mobility development.

References

[1] D. Cittanti, E. Vico and I. R. Bojoi, "New FOM-Based Performance Evaluation of 600/650 V SiC and GaN Semiconductors for Next-Generation EV Drives," in IEEE Access, vol. 10, pp. 51693-51707, 2022, doi: 10.1109/ACCESS.2022.3174777.J. Clerk Maxwell, A Treatise on Electricity and Magnetism, 3rd ed., vol. 2. Oxford: Clarendon, 1892, pp.68–73.

[2] D. C. Sheridan, D. Y. Lee, A. Ritenour, V. Bondarenko, J. Yang and C. Coleman, "Ultra-Low Loss 600V - 1200V GaN Power Transistors for High Efficiency Applications," PCIM Europe 2014; International Exhibition and Conference for Power Electronics, Intelligent Motion, Renewable Energy and Energy Management, Nuremberg, Germany, 20-22 May 2014, pp. 1-7.

[3] M. DONG, S. YIN, Y. WU and H. LI, "Performance Evaluation of 40-V/10-A GaN HEMT Versus Si MOSFET for Low-Voltage Buck Converter Application," 2020 IEEE 9th International Power Electronics and Motion Control Conference (IPEMC2020-ECCE Asia), Nanjing, China, 29 November 2020 - 02 December 2020, pp. 3428-3435, doi: 10.1109/IPEMC-ECCEAsia48364.2020.9367941..

[4] A. Lidow, M. De Rooij, J. Strydom, D. Reusch, J. Glaser. "GaN Transistors for Efficient Power Conversion," 3rd ed.; John Wiley & Sons: Hoboken, NJ, USA, 2019.

[5] D. K. Saini, A. Ayachit, M. K. Kazimierczuk and T. Suetsugu, "High switching frequency performance of E-GaN FETs and silicon MOSFETs," 2017 IEEE Industry Applications Society Annual Meeting, Cincinnati, OH, USA, 2017, pp. 1-6, doi: 10.1109/IAS.2017.8101846..

[6] S. Musumeci, V. Barba. "Gallium Nitride Power Devices in Power Electronics Applications: State of Art and Perspectives," Energies, 2023, 16(9), 3894. https://doi.org/10.3390/en16093894.

[7] 44. Faraci, G.; Rizzo, S.A.; Schembra, G. Unmanned aerial vehicles and wind generation serving isolated areas. In Proceedings of the 2020 International Symposium on Power Electronics, Electrical Drives, Automation and Motion (SPEEDAM), Sorren-to, Italy, 24–26 June 2020; pp. 138–143. https://doi.org/10.1109/SPEEDAM48782.2020.9161947

[8] S. Musumeci, F. Mandrile, V. Barba, and M. Palma, "Low-Voltage GaN FETs in Motor Control Application; Issues and Advantages: A Review," Energies, Vols. 14, no. 19: https://doi.org/10.3390/en14196378

[9] S. Musumeci, M. Palma, F. Mandrile and V. Barba, "Low-Voltage GaN Based Inverter for Power Steering Application," 2021 AEIT International Conference on Electrical and Electronic Technologies for Automotive (AEIT AUTOMOTIVE), Torino, Italy, 2021, pp. 1-6, doi: 10.23919/AEITAUTOMOTIVE52815.2021.9662703.

[10] 1. Meneghini, M.; De Santi, C.; Abid, I.; Buffolo, M.; Cioni, M.; Khadar, R.A.; Nela, L.; Zagni, N.; Chini, A.; Medjdoub, F.; et al. GaN-based power devices: Physics, reliability, and perspectives. J. Appl. Phys. 2021, 130, 181101. https://doi.org/10.1063/5.0061354.

[11] E. Armando, et al. "Low Voltage Trench-Gate MOSFETs for High Efficiency Auxiliary Power Supply Applications," 2019 International Conference on Clean Electrical Power (ICCEP), Otranto, Italy, 2019, pp. 165-170, doi: 10.1109/ICCEP.2019.8890217.

[12] J. S. Glaser and D. Reusch, "Comparison of deadtime effects on the performance of DC-DC converters with GaN FETs and silicon MOSFETs," 2016 IEEE Energy Conversion Congress and Exposition (ECCE), Milwaukee, WI, USA, 18-22 September 2016, pp. 1-8, doi: 10.1109/ECCE.2016.7854939.

[13] S. Musumeci, V. Barba, F. Mandrile, M. Palma and R. I. Bojoi, "Dead Time Reverse Conduction Investigation in GaN-Based Inverter for Motor Drives," IECON 2022 – 48th Annual Conference of the IEEE Industrial Electronics Society, Brussels, Belgium, 7-20 October 2022, pp. 1-6, doi: 10.1109/IECON49645.2022.9968787.

[14] F. Mandrile, S. Musumeci and M. Palma, "Dead Time Management in GaN Based Three-Phase Motor Drives," 2021 23rd European Conference on Power Electronics and Applications (EPE'21 ECCE Europe), Ghent, Belgium, 06-10 September 2021 2021, pp. P.1-P.10, doi: 10.23919/EPE21ECCEEurope50061.2021.9570665.